Journal of Physics and Chemistry of Solids 69 (2008) 2082–2090

Contents lists available at ScienceDirect

Journal of Physics and Chemistry of Solids

journal homepage: www.elsevier.com/locate/jpcs

Electrochemical behaviour of nano-sized spinel $LiMn_2O_4$ and $LiAl_xMn_{2-x}O_4$ (x = Al: 0.00–0.40) synthesized via fumaric acid-assisted sol–gel synthesis for use in lithium rechargeable batteries

R. Thirunakaran [a,*], A. Sivashanmugam [a], S. Gopukumar [a], Charles W. Dunnill [b], Duncan H. Gregory [b]

[a] Central Electrochemical Research Institute, Karaikudi 630 006, Tamil Nadu, India
[b] Chemistry Department, University of Glasgow, Joseph Black Building, Glasgow G12 8QQ, UK

ARTICLE INFO

Article history:
Received 21 August 2007
Received in revised form
28 February 2008
Accepted 5 March 2008

Keywords:
A. Inorganic compounds
A. Nanostructures
B. Sol-gel growth
C. X-ray diffraction
D. Electrochemical properties

ABSTRACT

Pristine spinel $LiMn_2O_4$ and $LiAl_xMn_{2-x}O_4$ (x = Al: 0.00–0.40) with sub-micron sized particles have been synthesized using fumaric acid as chelating agent by sol–gel method. The synthesized samples were subjected to thermogravimetric analysis (TGA), X-ray diffraction (XRD), Fourier transform infrared spectroscopy (FTIR), scanning electron microscopy (SEM), transmission electron microscopy (TEM) and cyclic voltammetry (CV) and galvanostatic cycling studies. The TGA curve of the gel shows several weight-loss regions stepwise amounting to 55% till 800 °C attributed to the decomposition of the precursors. Calcination to higher temperatures (800 °C) yields pure-phase spinel ($LiAl_xMn_{2-x}O_4$), as it is evident from the high-intensity XRD reflections matching to the standard pattern. SEM and TEM studies confirm that the synthesized grains are of uniform regular surface morphology. FT-IR studies show stretching and bending vibration bands of Li–O, Li–Al–Mn–O. $LiAl_{0.1}Mn_{1.90}O_4$ spinel was found to deliver discharge capacity of 139 mA h/g during the first cycle with columbic efficiency of 97%. $LiAl_{0.1}Mn_{1.90}O_4$ spinel exhibits the high cathodic peak current indicating better electrochemical performance. Low doping ($x = 0.1$) of Al is found to be beneficial in stabilizing the spinel structure.

1. Introduction

Pristine spinel $LiMn_2O_4$ is one of the most attractive candidates for rechargeable lithium batteries due to its low cost, non-toxic nature and ease of preparation when compared with other layered oxides such as $LiCoO_2$, and $LiNiO_2$ [1–3]. $LiCoO_2$ has many disadvantages such as high cost, not environmentally benign and low practical specific capacity against its theoretical value. The capacity of pure spinel $LiMn_2O_4$ upon repeated cycling diminishes at elevated temperature, which has been reported in several papers [4,5]. The capacity fading is caused due to several factors such as Jahn–Teller distortion, two-phase unstable reaction [2], slow dissolution of manganese into the electrolyte [6], lattice instability [7], and particle size distribution [8,9]. In order to suppress the Jahn–Teller distortion for obtaining the high cycling capacity during the repeated cycling, many researchers studied lithium-rich spinel with various divalent, trivalent and tetravalent-doped spinels such as Co, Zn, Cu, Fe, Ni, Cr, Ga, Ti, and Al [10], Ohzuku et al. [8], and Lee et al. [11], have reported earlier that partial doping of divalent and trivalent cations are more effective in suppressing the capacity fading up on cycling. Furthermore, the capacity fade of $LiMn_2O_4$ is often observed much in 3 V region which can be completely suppressed by doping selenium with $LiMn_2O_4$ [12]. Several low-temperature preparation methods viz., sol–gel method [13,14], chemical precipitation [15] pechini process and hydrothermal method [16] have been used to obtain cathode materials of required physical and electrochemical properties for rechargeable lithium-ion batteries.

Trivalent metal cation (Al^{3+}) was doped with $LiMn_2O_4$ partially to enhance the electrochemical stability by Masaki Yoshio et al. [17]. Oh et al. [6,18] reported that the spinel dissolution into the electrolyte resulting to electrochemical oxidation and polarization loss due to increase in cell resistance. Dahn et al. [19] reported the results of nickel-doped spinel compound under a variety of synthesis conditions. Strobel et al. [20] reported that $LiAl_xMn_{2-x}O_4$ and $LiMg_{0.5}Mn_{1.5}O_4$ materials seem to suppress the Jahn–Teller distortion in the Li–Mn–O system and further suggested that aluminium doping through solid solutions is easy, because it has ionic radius (Al^{3+} = 0.57 Å) closer to that of Mn^{3+} (0.66 Å). Al^{3+} ion doped in $LiNiO_2$ [21] was found to be beneficial in stabilization of nickel in the 3^+ oxidation state and suppress the capacity fading up on cycling. In this work, an attempt has been made for the first time to stabilize the $LiMn_2O_4$ spinel structure by "green chemistry method" using fumaric acid as chelating agent

* Corresponding author. Fax: +91 4565 227779.
E-mail address: rthirunakaran@yahoo.com (R. Thirunakaran).

0022-3697/$ - see front matter © 2008 Elsevier Ltd. All rights reserved.
doi:10.1016/j.jpcs.2008.03.009

with trivalent cation substitution ($LiAl_xMn_{2-x}O_4$: $x = Al$: 0.00–0.40). Sol–gel method provides many advantages such as sub-micron sized particles, regular morphology, low calcinations temperature, better homogeneity, nano-particle size, high surface area and good agglomeration nature when compared to solid-state synthesis [11].

2. Experimental

Pristine $LiMn_2O_4$ and $LiAl_xMn_{2-x}O_4$ ($x = Al$: 0.00–0.40) powders have been synthesized by sol–gel method using fumaric acid as chelating agent. Fig. 1 shows the flow chart of the synthesis procedure. Stoichiometric amounts of lithium acetate, manganese acetate, aluminium acetate and fumaric acid were mixed thoroughly and dissolved in de-ionized water. This solution was stirred continuously with gentle heating to get complete homogeneity. Fifty millilitres of 1 M fumaric acid was added to the highly homogenous solution and finally a thick gel was obtained. During stirring, the pH was maintained in the range 5–6. Fumaric acid facilitates formation of metal ligand chains between Mn–O and COO^- group resulting in the formation of pure spinel particles at relatively low temperature with superior morphological characteristics, which is essentially beneficial to obtain high electrochemical performance. From the obtained gel, small amount of samples were taken for TG/DTA to understand their thermal behaviour. The synthesized samples were dried overnight in an oven at 110 °C to remove the moisture and to obtain dried mass. The dried mass was ground and calcined at 800 °C for 4 h and subjected to various spectral and microscopic studies for physical characterization and finally for electrochemical studies.

2.1. Coin cell preparation

Coin cells of 2016 configuration were assembled in an argon filled glove box (MBraun, Germany) using lithium foil as anode, Celgard 2400 as separator, 1 M solution of $LiPF_6$ in 50:50 (v/v) mixture of ethylene carbonate (EC) and diethylene carbonate (DEC) as electrolyte and the synthesized compound as cathode material. The cathode mix consists of active material, carbon and poly (vinylidene fluride) PVdF binder in *N*-methyl-2-pyrrolidone (NMP) in the ratio 80:10:10. The slurry was coated over aluminium foil and vacuum dried at 110 °C for 2 h. The dried coating was pressed under 10 tonnes load for 2 min and the electrode blanks (diameter 18 mm) were punched out using a punching machine and used as cathode in the coin cell.

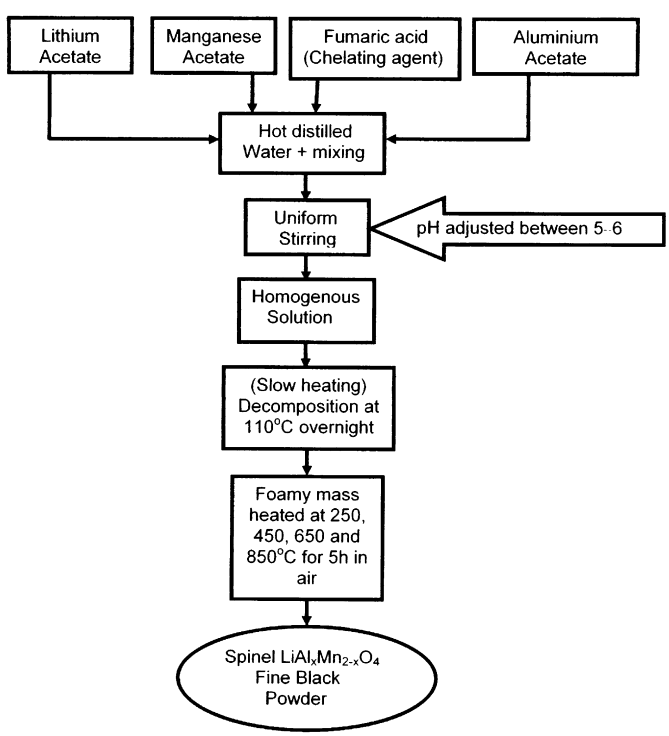

Fig. 1. Flow chart for synthesis of $LiAl_xMn_{2-x}O_4$ by sol–gel method using fumaric acid as chelating agent.

2.2. Electrochemical studies

The coin cells were cycled at a constant current of C/10 rate between 2.5 and 5.0 V in a battery cycling tester. Cyclic voltammograms of $LiMn_2O_4$ and $LiAl_xMn_{2-x}O_4$ were recorded at a sweep rate of 1 mV/s[1] against lithium foil as counter and reference electrode between the potential range 2.5–5.0 V.

3. Results and discussion

3.1. Thermal studies

Fig. 2 shows thermogravimetric analysis (TGA) of spinel $LiMn_2O_4$ precursor. The TG curve shows several weight-loss regions stepwise amounting to 55% till 800 °C. Up to 225 °C the sample loss less than 1% weight implies that the precursors do not contain any superficial or adsorbed water. A lucid weight-loss region starts from 225 °C extending up to 400 °C. This may be attributed to the initiation of the decomposition reaction towards the formation of $LiMn_2O_4$. This can be supplemented from the XRD results that the peak signatures of $LiMn_2O_4$ are indistinct for the as-synthesized and the calcined one at 250 °C. Characteristic peaks corresponding to $LiMn_2O_4$ spinel starts appearing after 450 °C. Further, the presence of impurity peaks in the XRD patterns corresponding to the calcined samples at 450 and 650 °C substantiate the progression of the reaction which is reflected in the TGA curve by way of the several weight-loss zones accounting to 20% until 700 °C. Gravimetrically stable region above 750 °C declares the completion of the reaction as can be corroborated by the striking similarity of the XRD peaks obtained for $LiMn_2O_4$ spinel calcined at 850 °C.

Fig. 3 depicts TGA curves of Al-doped ($x = Al$. $x = 0.10$, 0.20, 0.30 and 0.40) $LiAl_xMn_{2-x}O_4$ synthesized through fumaric acid-

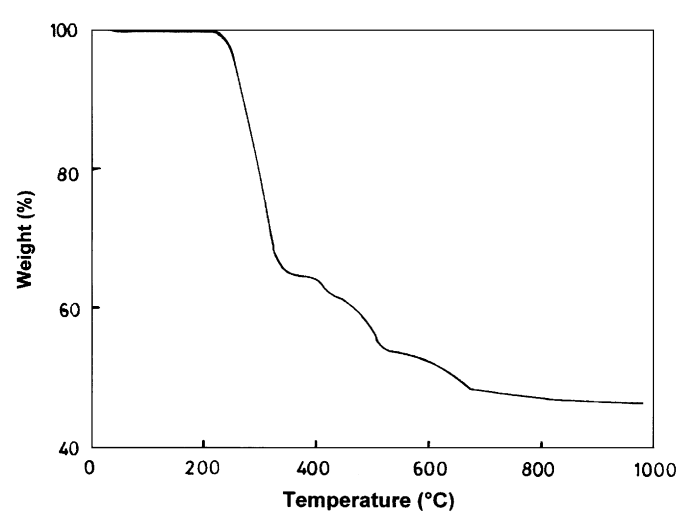

Fig. 2. Thermo gravimetric analysis (TGA) of spinel $LiMn_2O_4$ precursor.

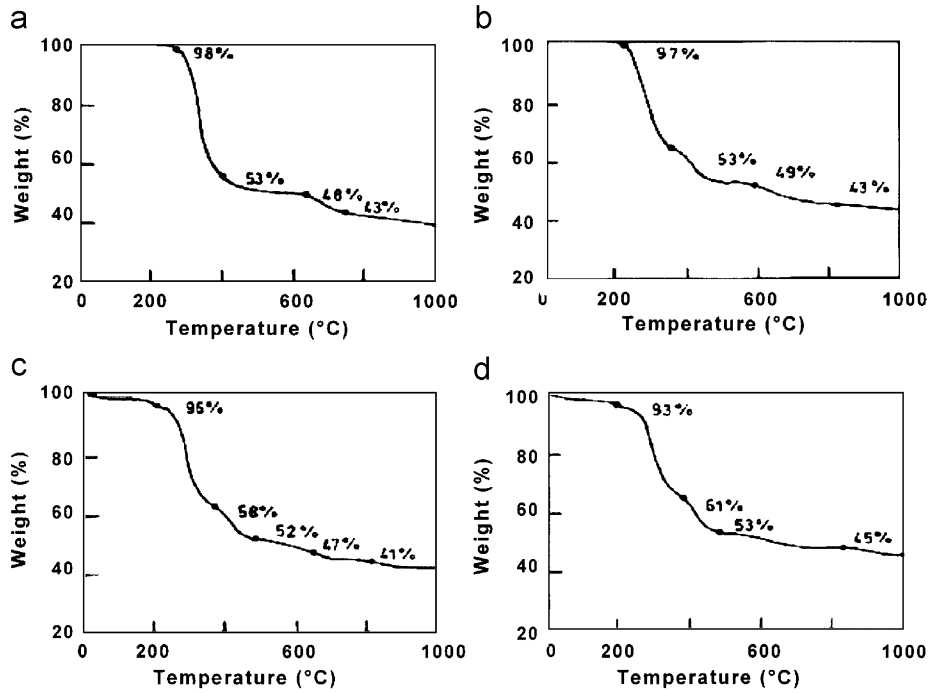

Fig. 3. Thermo gravimetric analysis (TGA) of $LiAl_xMn_{2-x}O_4$ precursor with different Al doping levels: (a) Al—0.10, (b) Al—0.20, (c) Al—0.30, (d) Al—0.40.

assisted sol–gel method. The thermal behaviour of Al-doped samples falls in line with that of the undoped $LiMn_2O_4$. Until 225 °C the sample loss less than 1% weight and afterwards the sample undergoes stepwise decomposition indicated by multiple weight-loss zones augmenting to 55% up to 700 °C. The reaction completes beyond 750 °C as can be inferred from the appearance of no weight-loss region.

3.2. X-ray diffraction

Fig. 4 shows the XRD patterns of as-synthesized and calcined $LiMn_2O_4$ samples at different temperatures viz., 250, 450, 650 and 850 °C. The XRD patterns for the as-synthesized shows fairly weak reflections with few impurity peaks indicating the highly amorphous nature of the product. The additional peaks corresponding to α-Mn_2O_3 and $LiMn_2O_3$ were observed for the low-heated (250 and 450 °C) samples. Upon calcination, the phase purity gets improved as can be seen from the pattern obtained for the calcined one at 250 °C, wherein the characteristic peak signatures start appearing. Calcination at higher temperatures yields phase-pure spinel as it is evident from the high-intensity XRD reflections obtained for the samples calcined at 800 °C corresponding to the planes (111), (311), (222), (400), (331), (551), (440), (531) and (222), respectively. These observations are in good agreement with the earlier reports [22–24]. $LiMn_2O_4$ spinel belongs to Fd3m symmetry, wherein the manganese ions occupy 16d sites and oxygen ions occupy 32e sites.

Fig. 5 shows the XRD patterns of the undoped and Al-doped ($x = Al$: $x = 0.10$, 0.20, 0.30 and 0.40) $LiMn_2O_4$ synthesized through fumaric acid-assisted sol–gel method and calcined at 850 °C. All the peaks signatures of the XRD pattern for $LiMn_2O_4$ and $LiAl_xMn_{2-x}O_4$ confirm to JCPDS card No-35-782 corresponding to single-phase spinel compound without any impurities. It is in good agreement with that of previous work [25,26]. It is evident that fumaric acid as a chelating agent forms metal ligands easily between Mn–O and COO^- group resulting in the easy formation of the product which can be substantiated by the matching reflections observed in the XRD pattern.

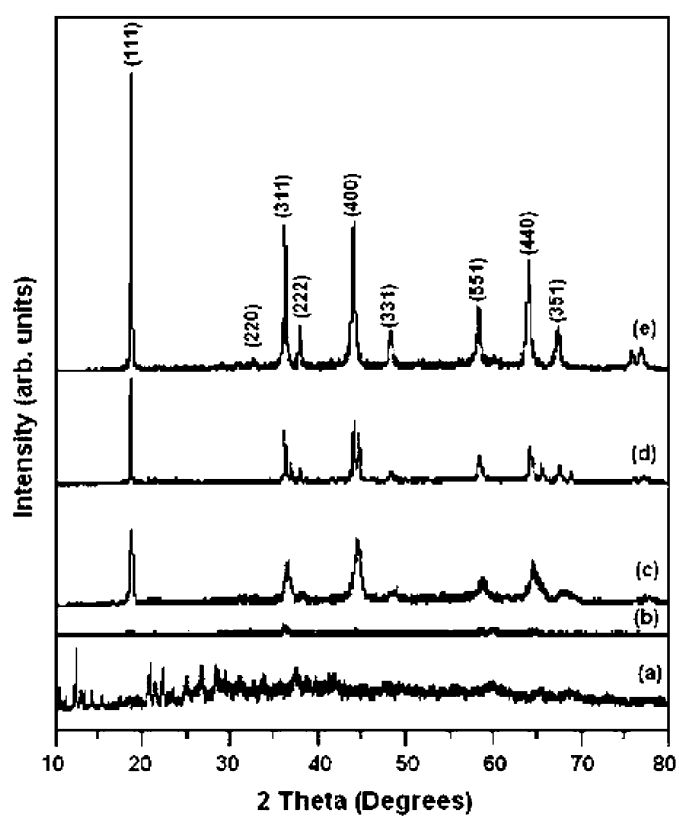

Fig. 4. XRD patterns of sol–gel-synthesized $LiMn_2O_4$ samples calcined at different temperatures: (a) as-synthesized, (b) 250 °C, (c) 450 °C, (d) 650 °C, (e) 850 °C.

3.3. Scanning electron microscopy

SEM studies reflect the textural and morphological characteristics of the synthesized material. Fig. 6 shows the SEM images of spinel $LiMn_2O_4$ particles calcined at different temperatures (250, 450, 650 and 850 °C). It can be seen that the particles of the $LiMn_2O_4$ powders calcined at 250 °C are in the order 200–500 nm. Further, upon calcination the grain size of the particles grow bigger. $LiMn_2O_4$ powders calcined at 850 °C are of micron size showing irregular morphology. Fig. 7 shows the SEM images of sol–gel derived $LiAl_xMn_{2-x}O_4$ powders with different Al stoichiometry viz., $x = 0.10$, 0.20, 0.30 and 0.40 calcined at 850 °C. It is interesting to note that the particles are of spherical grains even at high calcination temperature (850 °C) for all the samples. Uniformly the grains appear as agglomerated clusters at all concentrations of aluminium. The average grain size is less than 300 nm. The order of agglomeration appears to increase meagrely with high Al doping.

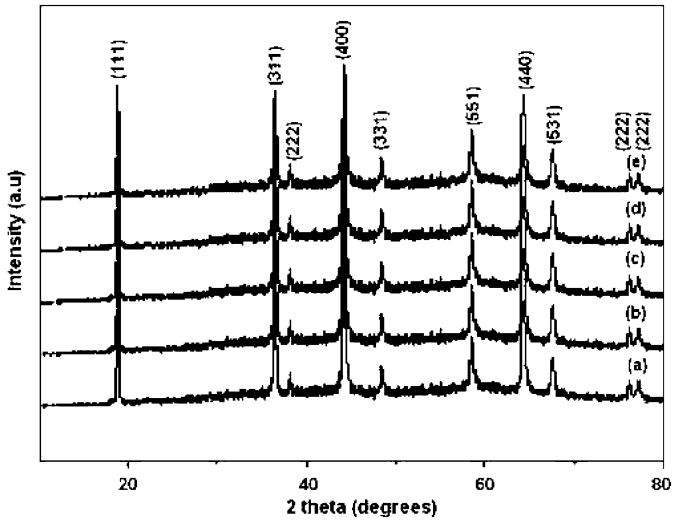

Fig. 5. XRD patterns of $LiMn_2O_4$ and $LiAl_xMn_{2-x}O_4$ with varying Al doping calcined at 850 °C: (a) Al—0.00, (b) Al—0.10, (c) Al—0.20, (d) Al—0.30, (e) Al—0.40.

3.4. Transmission electron microscopy

Fig. 8 shows TEM images of spinel $LiMn_2O_4$ particles calcined at different temperatures (250, 450, 650 and 850 °C). It is clear that with increased calcination temperature results in agglomeration of the particles. Fig. 9 shows TEM images of sol–gel derived $LiAl_xMn_{2-x}O_4$ powders with different Al stoichiometry viz., $x = 0.10$, 0.20, 0.30 and 0.40 calcined at 850 °C. Here also, it could be seen that the samples with higher aluminium contents appears to be more cohesive in nature, which would be more useful to derive better electrochemical performance.

3.5. FTIR spectroscopy

The spectroscopic studies on chromium-doped spinel $LiMn_2O_4$ for lithium-ion batteries have been investigated by Xuejie Huang et al. [27]. FTIR study on aluminium-doped $LiNiO_2$ has been investigated by Kalyani et al. [21]. Fig. 10 shows FTIR spectra of sol–gel derived $LiMn_2O_4$ powders calcined at different temperatures viz., 250, 450, 650 and 850 °C. The details of wavenumber

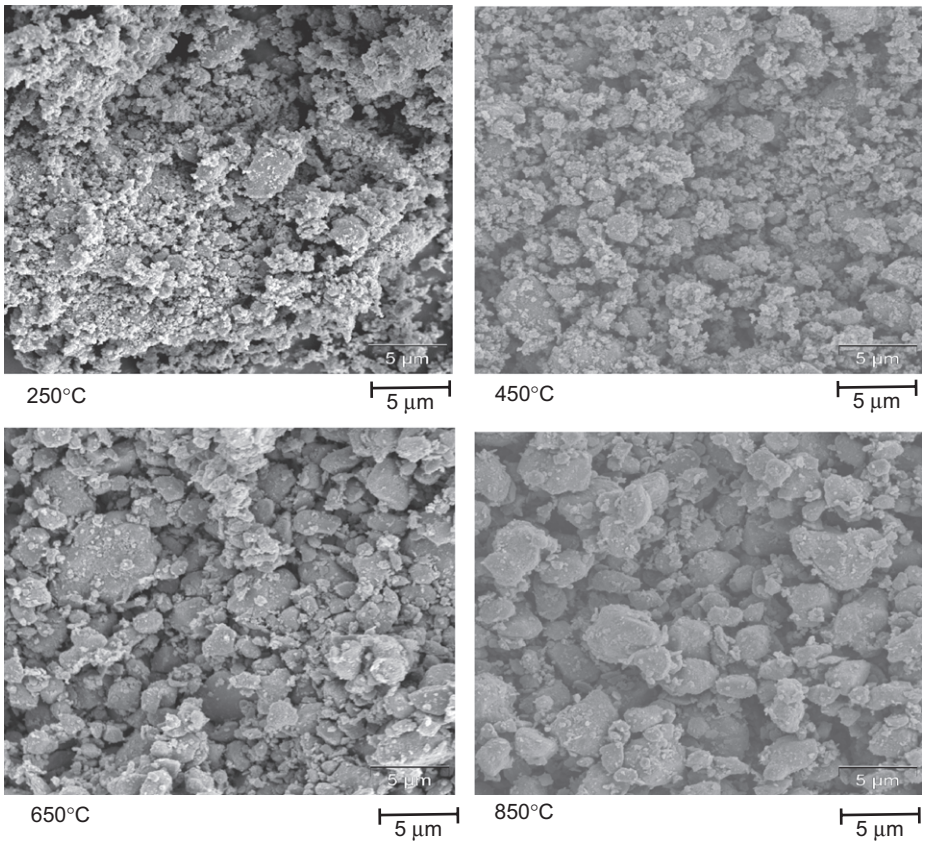

Fig. 6. SEM images of spinel $LiMn_2O_4$ particles calcined at different temperatures viz., 250, 450, 650 and 850 °C.

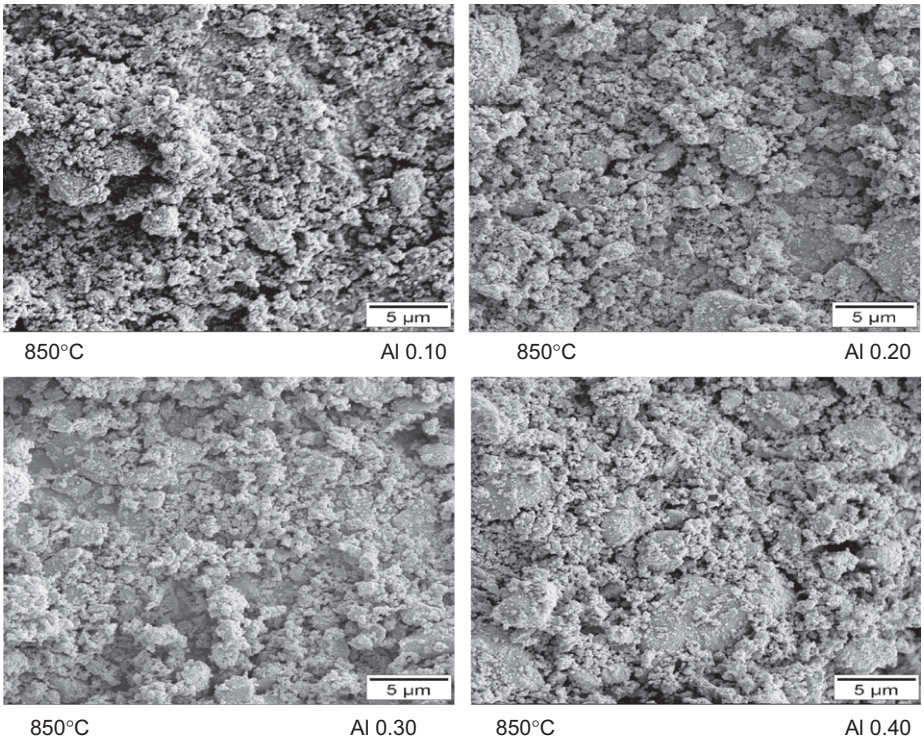

Fig. 7. SEM images of $LiAl_xMn_{2-x}O_4$ particles with varying Al doping calcined at 850 °C: (a) Al—0.10, (b) Al—0.20, (c) Al—0.30, (d) Al—0.40.

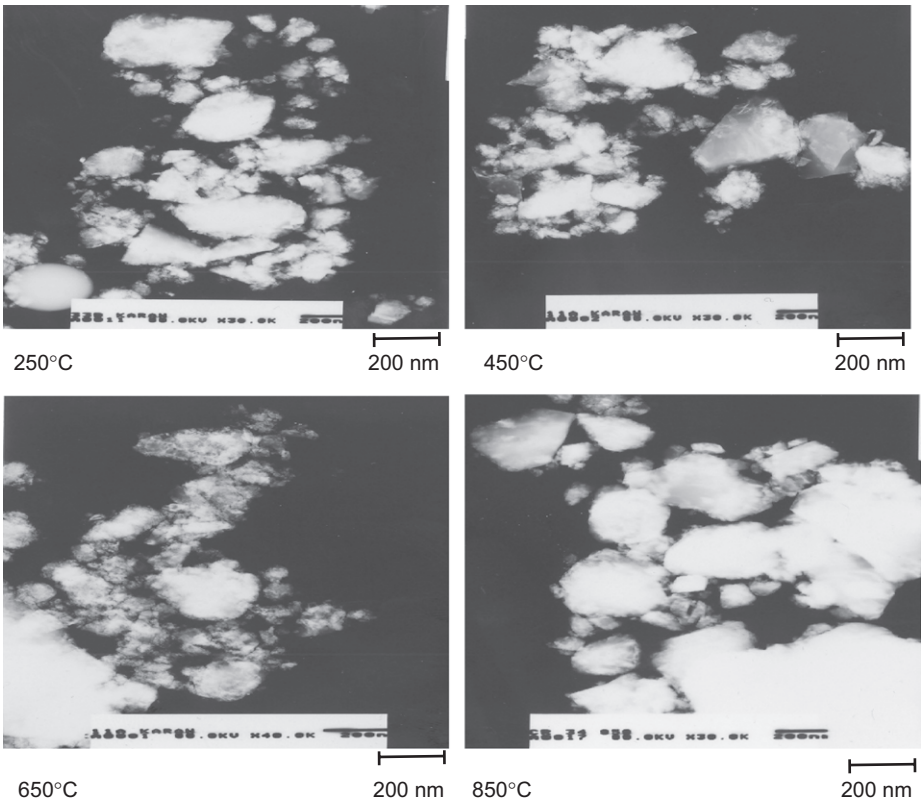

Fig. 8. TEM images of spinel $LiMn_2O_4$ particles calcined at different temperatures viz., 250, 450, 650 and 850 °C.

corresponding to $LiMn_2O_4$ and $LiAl_xMn_{2-x}O_4$ powders are presented in Tables 1 and 2, respectively. The IR spectral bands present in lower wavelength around 1670 cm^{-1} may be ascribed to Li–O bending vibration mode and the peaks around 3475 cm^{-1} is attributed to Li–Mn–O stretching vibration band. These observations are in agreement with that of previous results [28].

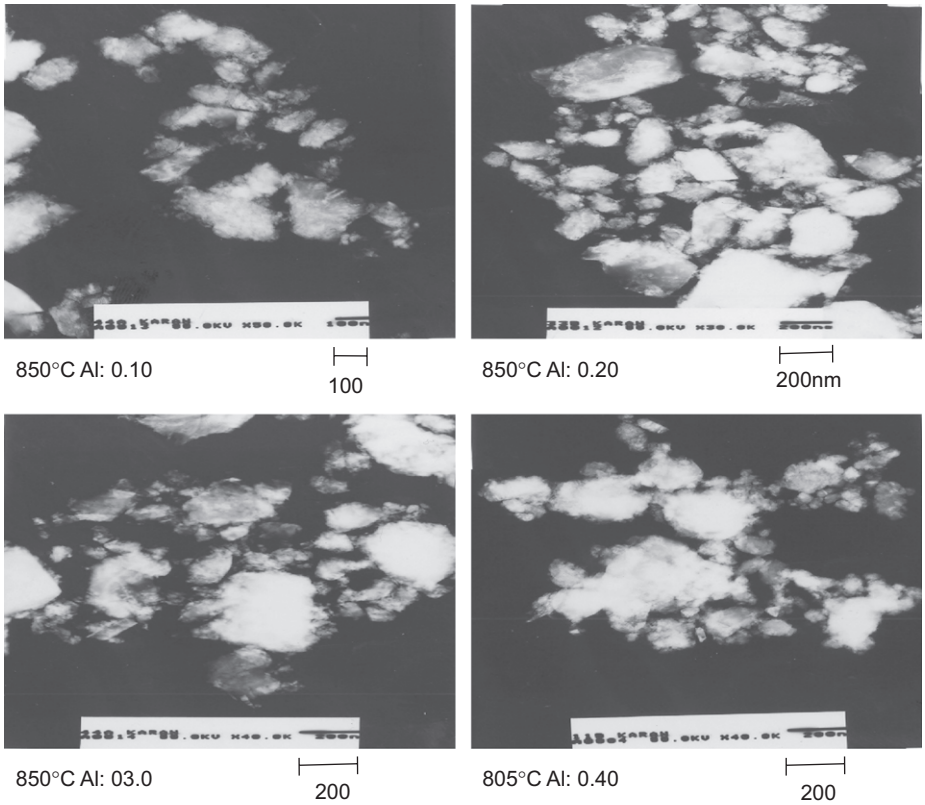

Fig. 9. TEM images of $LiAl_xMn_{2-x}O_4$ particles with varying Al doping calcined at 850 °C: (a) Al—0.10, (b) Al—0.20, (c) Al—0.30, (d) Al—0.40.

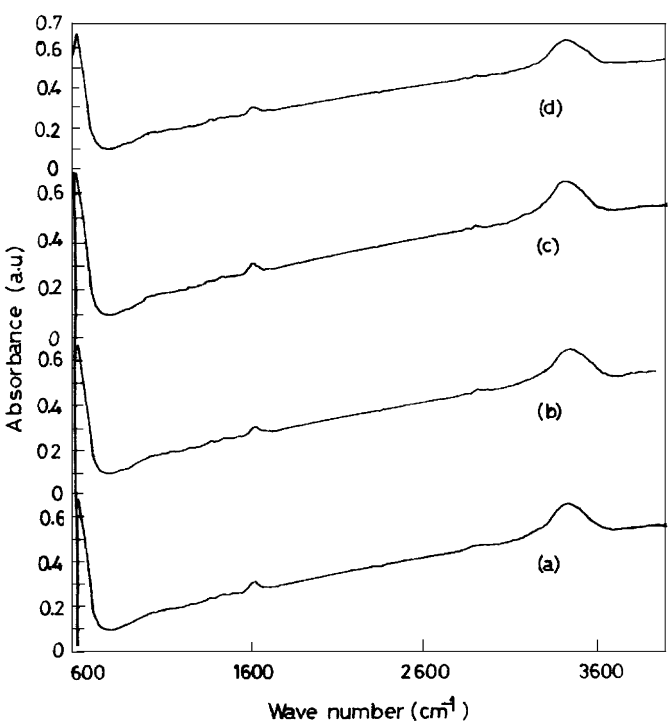

Fig. 10. FTIR spectra of spinel $LiMn_2O_4$ particles calcined at different temperatures viz., 250, 450, 650 and 850 °C.

Table 1
FTIR frequencies for the peaks observed for $LiMn_2O_4$

No	Temperature (°C)	Wave number (cm^{-1})	Assignments
1	250	1670	Li–O
		3475	Li–Mn–O
2	450	1658	Li–O
		3469	Li–Mn–O
3	650	1652	Li–O
		3460	Li–Mn–O
4	850	1638	Li–O
		3453	Li–Mn–O

Table 2
FTIR frequencies for the peaks observed for $LiAl_xMn_{2-x}O_4$

No	Temperature (°C)	(Al-level)	Wave number (cm^{-1})	Assignments
1	850	0.10	1659	Li–O
			3468	Li–Al–Mn–O
2	850	0.20	1658	Li–O
			3454	Li–Al–Mn–O
3	850	0.30	1652	Li–O
			3445	Li–Al–Mn–O
4	850	0.40	1640	Li–O
			3436	Li–Al–Mn–O

It is clear that the spectral reflections have no significant influence over the calcination temperature, as the observed spectrum appears similar in all the cases except a slight shift towards lower wavenumber. Fig. 11 shows the spectra of the sol–gel derived $LiAl_xMn_{2-x}O_4$ powders with different Al stoichiometry viz., $x = 0.10$, 0.20, 0.30 and 0.40 calcined at 850 °C. The IR spectral

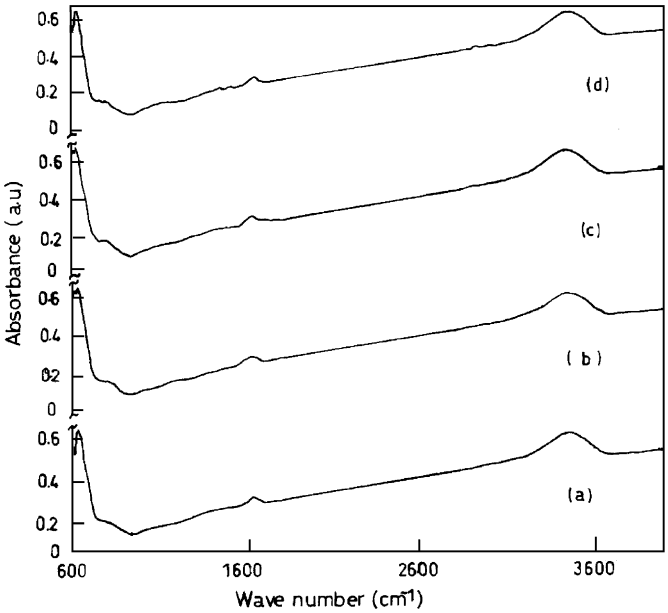

Fig. 11. FTIR Spectra of $LiAl_xMn_{2-x}O_4$ particles with varying Al doping calcined at 850 °C: (a) Al—0.10, (b) Al—0.20, (c) Al—0.30, (d) Al—0.40.

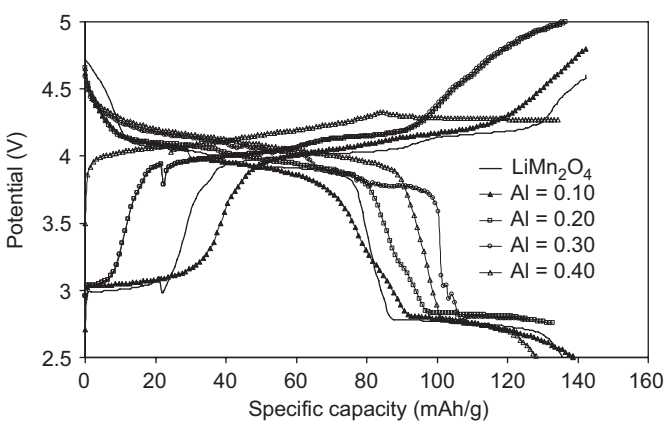

Fig. 12. Charge–discharge behaviour of $LiMn_2O_4$ and $LiAl_xMn_{2-x}O_4$ with varying Al doping viz., 0.10, 0.20, 0.30 and 0.40 calcined at 850 °C.

bands present in lower wavenumber around 1659 cm^{-1} may be ascribed to Li–O bending vibration mode and the peaks around 3468 cm^{-1} is attributed to Li–Al–Mn–O stretching vibration band.

3.6. Charge– discharge studies

Structurally $LiMn_2O_4$ has been refined with space group Fd3m, which can be described as layers of close-packed oxygen atoms, in which lithium and manganese ions occupy tetrahedral (8a) and octahedral (16d) sites, respectively. The basic electrochemical process involves the removal of Li ions from 8a tetrahedral sites during charging in the 4 V region, and $LiMn_2O_4$ transforms into λ-MnO_2 which is also having a cubit unit cell. During charge upto 3 V, Li ions are inserted into the 16d octahedral, and $Li_2Mn_2O_4$ with a tetragonal lattice is formed. A fundamental problem prohibiting a wider use of the Mn spinel as a 4 V cathode for lithium-ion batteries is the remarkable capacity fade at elevated temperatures. Doping with foreign metal ions, like Mg^{2+}, Ga^{3+}, Al^{3+}, Ni^{2+}, Cu^{2+}, Co^{2+}, Cr^{3+} and Fe^{2+} has been suggested to stabilize its structure. The doping ions substitute for Mn^{3+} and so they reduce the capacity delivered at 4 V. Further, doping results in manganese oxidation state approaching 4^+ and lithium insertion into its structure occurs below 3.0 V [29–31]. In the present investigations Al-doped $LiMn_2O_4$ samples were cycled between 2.5 and 5.0 V. First cycle charge–discharge curves of sol–gel derived $LiMn_2O_4$ and $LiAl_xMn_{2-x}O_4$ powders with different Al stoichiometry viz., $x = 0.10$, 0.20, 0.30 and 0.40 calcined at 850 °C and their cycling performance curves over 10 cycles, and their corresponding columbic efficiencies (CE) are presented in Figs. 12 and 13. Undoped-spinel $LiMn_2O_4$ calcined at 850 °C delivered discharge capacity around 135 mA h/g against the charge capacity of 145 mA h/g corresponding to 93% CE during the first cycle. These cells show a fading cycling feature. In the 10th cycle these cells deliver 94 mA h/g amounting to capacity fade of 3% per cycle.

In the case of Al-doped spinels, it is interesting to note that, a slight decrease in charge–discharge performance is observed when compared to undoped $LiMn_2O_4$. Further, 0.1 Al stoichiometry exhibits discharge capacity of 139 mA h/g, whereas the same is 128 mA h/g for 0.4Al. It is apparent that high degree of Al doping results in lowering of discharge capacity [32]. It may not be denied that high doping might have led to a possible cation mixing thereby causing a short-range structural disorder. While considering the cycling stability and CE low-order doping of aluminium is found to be beneficial. $LiAl_{0.1}Mn_{1.9}O_4$ electrodes deliver discharge capacity of 139 mA h/g against the charge capacity of 142 mA h/g yielding 97% CE during the first cycle. These cells show a slow-fading cycling behaviour. Over the 10 cycles these cells deliver 97 mA h/g amounting to capacity fade of 3% per cycle. The capacity fade increases to 3.5%, 3.6% and 3.7% per cycle upon increase in Al content to 0.2, 0.3 and 0.4, respectively. The capacity retention of higher stoichiometry aluminium-doped spinel fall down drastically except $LiAl_{0.10}Mn_{1.90}O_4$. Lee et al. [17] reported 121 mA h/g as first-cycle discharge capacity with 0.09Al, whereas the present study reveals 139 mA h/g with 0.1 Al. Over the 10 cycles also the present study has shown slightly superior performance of 97 mA h/g. Bao et al. [33] has also studied $LiAl_{0.10}Mn_{1.90}O_4$ derived through micro wave-assisted sol–gel synthesis and reported initial discharge capacity of 122 mA h/g [33]. Certainly, the present method of fumaric acid-assisted sol–gel preparation facilitates the formation of metal ligand chains between Mn–O and COO^- group resulting in the formation of pure spinel particles at relatively low temperature with superior morphological characteristics, which essentially ensuing to superior electrochemical performance as is evident from the higher discharge capacity (139 mA h/g) obtained for ($LiAl_{0.1}Mn_{1.90}O_4$) when compared to the previous reports [17,33].

3.7. Cyclic voltammetry

Cyclic voltammogram of $LiMn_2O_4$ obtained for the first cycle in the potential range 2.5–5.0 V using Li as reference and counter-electrode at a scan rate of 1 mV/s^1 is presented in Fig. 14(a). A single broad anodic peak observed at 4.5 V is corresponding to the extraction of lithium ions and the single broad cathodic peak at 3.5 V is associated to the insertion of lithium ions from and to the spinel structure [24,34]. Fig. 14(b) depicts cyclic voltammogram of

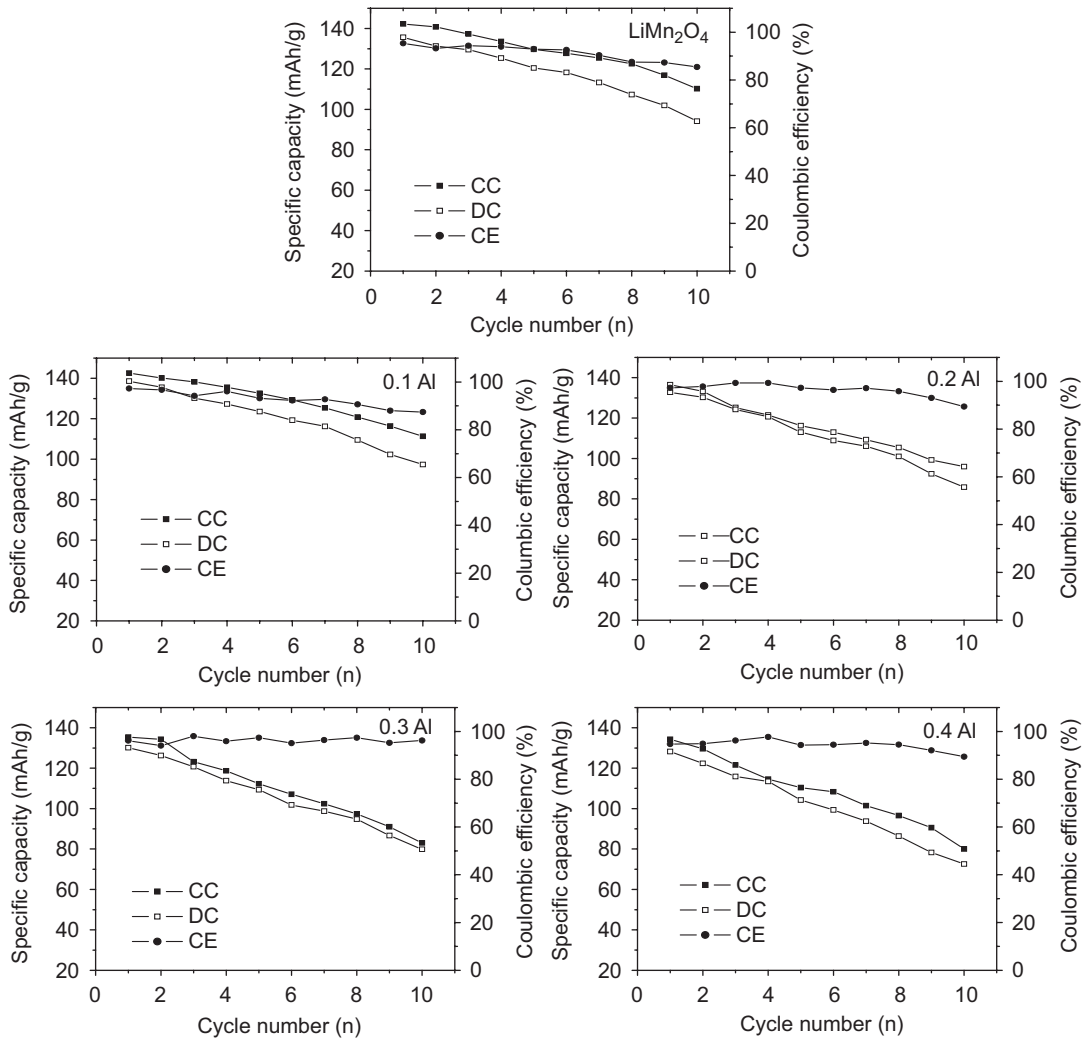

Fig. 13. Cycling behaviour of $LiMn_2O_4$ and $LiAl_xMn_{2-x}O_4$ with varying Al doping viz., 0.10, 0.20, 0.30 and 0.40 calcined at 850 °C. CC—charge capacity, DC—discharge capacity; CE—columbic efficiency.

$LiAl_{0.10}Mn_{1.90}O_4$ obtained for the first cycle in the potential range 2.5–5.0 V using Li as reference and counterelectrode at a scan rate of 1 mV/s[1]. Unlike pristine $LiMn_2O_4$, the Al-doped spinel particles exhibit lithium extraction during the oxidative sweep in two potential regions around 3.3 and 4.5 V. and in the reductive sweep lithium insertion occurs over a broad potential range (4.5–3.0 V). In Al-doped spinel, lithium ions can intercalate/deintercalate through the three-dimensional vacant channels formed by cubic close-packed array of oxygen ions into the tetrahedral sites (8a), which share face with vacant octahedral sites (16c) during the electrochemical reaction. Further, it has been reported [11] that the reversibility of $LiMn_2O_4$ could be improved by doping various metal cations such as Co^{2+}, Ni^{2+}, Mg^{2+}, Cr^{3+}, etc. In the case of cyclic voltammogram of $LiAl_{0.10}Mn_{1.90}O_4$, the anodic and cathodic peaks are relatively well defined and sharp indicating that the powder exhibits high crystallinity [35–37], which is supplemented from the high-intensity XRD reflections obtained for Al-doped samples (Fig. 5) than the parent compound. The high structural ordering of Al-doped spinel is reflected through higher peak currents observed for Al-doped spinel vindicate its superior electrochemical performance when compared to the parent $LiMn_2O_4$.

4. Conclusions

Using fumaric acid as a new chelating agent $LiAl_xMn_{2-x}O_4$ ($x = 0.0$–0.40) spinel structured compounds were synthesized from lithium acetate, manganese acetate and aluminium acetate as starting materials in a simple sol–gel procedure. The synthesized materials were subjected to TGA, PXRD, SEM, TEM, and FT-IR studies to ascertain the physical properties. The TGA curve of the gel shows several weight-loss regions stepwise amounting to 55% till 800 °C attributed to the decomposition of the precursors. Calcination to higher temperatures (850 °C) yield phase-pure spinel ($LiAl_xMn_{2-x}O_4$) as it is evident from the high-intensity XRD reflections matching to the standard. SEM and TEM studies confirm that the synthesized grains are of uniform regular surface morphology. FT-IR studies confirm the stretching and bending vibration bands of Li–O, Li–Al–Mn–O. $LiAl_{0.1}Mn_{1.90}O_4$ spinel was found to deliver discharge capacity of 139 mA h/g during the first cycle with CE of 97%. $LiAl_{0.1}Mn_{1.90}O_4$ spinel exhibits the high cathodic peak current indicating better electrochemical performance. Low doping ($x = 0.1$) of Al is found to be beneficial in stabilizing the spinel structure.

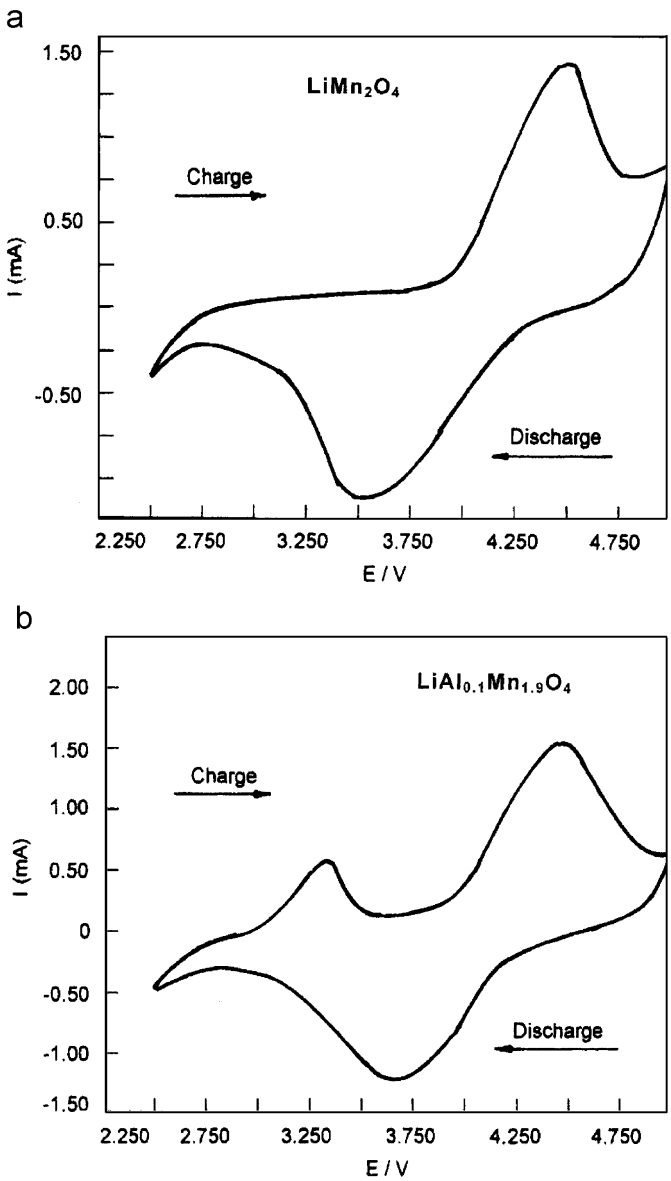

Fig. 14. Cyclic voltammogram of (a) $LiMn_2O_4$, and (b) $LiAl_{0.10}Mn_{1.90}O_4$.

Acknowledgements

Dr. R. Thirunakaran acknowledges Royal Society, London for awarding the Post Doctoral Fellowship and thankful to Prof. Duncan Gregory to pursue research work under his guidance at the Chemistry Department, University of Glasgow. He also thanks Dr. Emina Hadzifejzovic and Dr. Jinhan Yao for their great help during his stay in Glasgow. Dr. R. Thirunakaran is also thankful to Prof. A. K. Shukla, Director, CECRI and CSIR for granting leave to avail the above fellowship.

References

[1] J.M. Tarascon, W.R. McKinnon, F. Coowar, T.N. Bowner, G. Amatucci, D. Guyomard, J. Electrochem. Soc. 141 (1994) 1421.
[2] R.J. Gummow, A. de Kock, M.M. Thackeray, Solid State Ionics 69 (1994) 59.
[3] M.M. Thackeray, A. de Kock, M.H. Rossouw, D. Liles, R. Bittihn, D.J. Hoge, J. Electrochem. Soc. 139 (1992) 363.
[4] Y. Xia, M.J. Yoshio, J. Electrochem. Soc. 144 (1977) 2593.
[5] G. Pistoia, A. Antonini, R. Rosati, D. Zane, Electrochim. Acta 41 (1996) 2683.
[6] D.H. Jang, J.Y. Shin, S.M. Oh, J. Electrochem. Soc. 143 (1996) 2204.
[7] A. Yamada, J. Solid State Chem. 122 (1996) 160.
[8] T. Ohzuku, S. Takeda, M. Iwanaga, J. Power Sources 82 (1999) 90.
[9] D. Song, H. Ikuta, T. Uchida, M. Wakihara, Solid State Ionics 117 (1999) 151.
[10] M. Javed Iqbal, S. Zahoor, J. Power Sources 165 (2007) 393.
[11] J.H. Lee, J.K. Hong, D.H. Jang, Y.K. Sun, S.M. Oh, J. Power Sources 89 (2000) 7.
[12] S.H. Park, K.S. Park, Y.K. Sun, K.S. Nahm, J. Electrochem. Soc. 147 (2000) 2116.
[13] S. Bach, M. Henry, N. Baffier, J. Livage, J. Solid State Chem. 88 (1990) 325.
[14] J.P. Perreira-Ramos, J. Power Sources 54 (1995) 120.
[15] P. Barboux, J.M. Tarascon, F.K. Shokoohi, J. Solid State Chem. 94 (1991) 185.
[16] W. Liu, G.C. Farrington, F. Chaput, B.J. Dunn, J. Electrochem. Soc. 143 (1996) 879.
[17] Y.S. Lee, N. Kumada, M. Yoshio, J. Power Sources 96 (2001) 376.
[18] D.H. Jang, Y.J. Shin, S.M. Oh, J. Electrochem. Soc. 144 (1997) 3342.
[19] Q. Zhone, A. Bonakdarpour, M. Zhang, Y. Gao, J.R. Dahn, J. Electrochem. Soc. 144 (1997) 205.
[20] F. Le Cras, D. Bloch, M. Anne, P. Strobel, Solid State Ionics 203 (1996) 203.
[21] P. Kalyani, N. Kalaiselvi, N. Muniyandi, J. Electrochem. Soc. 150 (2003) 759.
[22] D. Shu, S. Gopukumar, K.B. Kim, K.S. Ryu, S.H. Chang, Solid State Ionics 160 (2003) 227.
[23] X. Wang, X. Chen, L. Gao, H. Zhenug, M. Ji, T. Shen, Z. Zhang, J. Cryst. Growth 256 (2003) 123.
[24] R. Thirunakaran, K.T. Kim, Y.M. Kang, C.Y. Seo, J.Y. Lee, J. Power Sources 137 (2004) 100.
[25] Y.S. Lee, N. Kumada, M. Yoshio, J. Power Sources 96 (2001) 376.
[26] G.T.K. Fey, C.Z. Lu, T. Premkumar, Mater. Chem. Phys. 80 (2003) 309.
[27] C. Wu, Z. Wang, F. Wu, L. Chen, X. Huang, Solid State Ionics 144 (2001) 277.
[28] Y.M. Hon, S.P. Lin, K.Z. Fung, M.H. Hon, J. Eur. Ceram. Soc. 22 (2002) 653.
[29] M.M. Thackeray, A. De Kock, Mater. Res. Bull. 28 (1993) 1041.
[30] M.H. Rossouw, A. De Kock, L.A. De Picciotto, M.M. Thackeray, Mater. Res. Bull. 25 (1990) 173.
[31] A. De Kock, M.H. Rossouw, L.A. Picciotto, M.M. Thackeray, Mater. Res. Bull. 25 (1990) 657.
[32] J.Y. Luo, X.L. Li, Y.Y. Xia, Electrochim. Acta 52 (2007) 4525.
[33] S.J. Bao, Y. Liang, W.J. Zhou, B.L. He, H.L. Li, J. Power Sources 154 (2006) 239.
[34] R.H. Zeng, W.S. Li, D.S. Lu, Q.M. Huang, J. Power Sources 174 (2007) 592.
[35] N. Santander, S.R. Das, S.B. Majumder, R.S. Katiyar, Surf. Coat. Technol. 177/178 (2004) 60.
[36] B.H. Kim, Y.K. Choi, Y.H. Choa, Solid State Ionics 158 (2003) 281.
[37] W.J. Zhou, S.J. Bao, B.L. He, Y.Y. Liang, H.L. Li, Electrochim. Acta 22 (2006) 4708.